Endothelial depletion of murine SRF/MRTF provokes intracerebral hemorrhagic stroke

Christine Weinl[a,1], Salvador Castaneda Vega[b], Heidemarie Riehle[a], Christine Stritt[a], Carsten Calaminus[b], Hartwig Wolburg[c], Susanne Mauel[d], Angele Breithaupt[d], Achim D. Gruber[d], Bohdan Wasylyk[e,f,g,h], Eric N. Olson[i,1], Ralf H. Adams[j], Bernd J. Pichler[b], and Alfred Nordheim[a,1]

[a]Department of Molecular Biology, Interfaculty Institute of Cell Biology, University of Tuebingen, 72076 Tuebingen, Germany; [b]Werner Siemens Imaging Center, Department of Preclinical Imaging and Radiopharmacy, University Hospital Tuebingen, 72076 Tuebingen, Germany; [c]Department of Pathology and Neuropathology, University of Tuebingen, 72076 Tuebingen, Germany; [d]Institute for Animal Pathology, Department of Veterinary Pathology, Free University Berlin, 14163 Berlin, Germany; [e]Institut de Génétique et de Biologie Moléculaire et Cellulaire, 67400 Illkirch, France; [f]Centre National de la Recherche Scientifique, UMR 7104, 67404 Illkirch, France; [g]Institut National de la Santé et de la Recherche Médicale, U964, 67400 Illkirch, France; [h]Université de Strasbourg, 67400 Illkirch, France; [i]Department of Molecular Biology, University of Texas Southwestern Medical Center, Dallas, TX 75390; and [j]Department of Tissue Morphogenesis, Max-Planck-Institute for Molecular Biomedicine and Faculty of Medicine, University of Muenster, 48149 Muenster, Germany

Contributed by Eric N. Olson, July 2, 2015 (sent for review May 5, 2015)

Intracerebral hemorrhagic stroke and vascular dementia are age- and hypertension-associated manifestations of human cerebral small vessel disease (SVD). Cerebral microvessels are formed by endothelial cells (ECs), which are connected through tight junctions, adherens junctions, and stabilizing basement membrane structures. These endothelial connections ensure both vessel stability and blood–brain barrier (BBB) functions, the latter enabling selective exchange of ions, bioactive molecules, and cells between the bloodstream and brain tissue. *Srf*^{iECKO} mice, permitting conditional EC-specific depletion of the transcription factor Serum Response Factor (SRF), suffer from loss of BBB integrity and intracerebral hemorrhaging. Cerebral microbleeds and larger hemorrhages developed upon postnatal and adult depletion of either SRF or its cofactors Myocardin Related Transcription Factor (MRTF-A/-B), revealing essential requirements of ongoing SRF/MRTF activity for maintenance of cerebral small vessel integrity. In vivo magnetic resonance imaging allowed detection, localization, and time-resolved quantification of BBB permeability and hemorrhage formation in *Srf*^{iECKO} brains. At the molecular level, direct and indirect SRF/MRTF target genes, encoding structural components of tight junctions (Claudins and ZO proteins), adherens junctions (VE-cadherin, α-Actinin), and the basement membrane (Collagen IV), were down-regulated upon SRF depletion. These results identify SRF and its MRTF cofactors as major transcriptional regulators of EC junctional stability, guaranteeing physiological functions of the cerebral microvasculature. We hypothesize that impairments in SRF/MRTF activity contribute to human SVD pathology.

blood–brain barrier | cerebral microbleeds | conditional gene knockout | stroke mouse model | transcription

Stroke causes more than one of every 20 human deaths in the United States, whereby stroke pathology presents as ischemic (87%), intracerebral hemorrhagic (10%), or subarachnoid hemorrhagic (3%) (1). Intracerebral hemorrhage is a component of human cerebral small vessel disease (SVD), an age- and hypertension-associated cerebral morbidity with increasing incidence, occurring in familial and sporadic manifestations (2). Intracerebral hemorrhage displays lesions of variable volume, including macro- and microhemorrhages (microbleeds), readily visualized by magnetic resonance imaging (MRI) (3). Microbleeds are considered indicators of intracerebral hemorrhage risk in stroke medicine (4).

The cerebral microvasculature is built by endothelial cell (EC) interactions, involving tight junctions, adherens junctions, and EC basement membrane structures, thereby forming the blood–brain barrier (BBB) of capillaries for selective exchange between the blood and the brain parenchyme (for review, see refs. 2, 3, and 5).

Serum Response Factor (SRF), a ubiquitously expressed transcription factor, activates expression of target genes dependent upon recruitment of one of at least two classes of cofactors, the Ternary Complex Factors (TCFs) or the Myocardin Related Transcription Factors (MRTFs) (6–9). Previously, by using *Srf*^{iECKO} and *Mrtf-a*$^{(-/-)}$*Mrtf-b*^{iECKO} mice, an endothelial role of murine SRF and its MRTF cofactors was shown for retinal angiogenesis (10, 11).

The above inducible mouse lines were used to analyze the cerebral vasculature in detail. Depletion of SRF or MRTF-A/-B at postnatal days induced cerebral hemorrhages at early postnatal age. Similarly, adult depletion of SRF caused *Srf*^{iECKO} animals to develop symptoms characteristic of SVD associated with cerebral hemorrhagic stroke. With time, brain hemorrhages increased progressively in number and were observed in all brain areas. MRI identified multiple perivascular blood extravasations of variable size and allowed lesion localization and quantitation. MRI further indicated vessel leakiness before the formation of blood-borne hemosiderin deposits. Structural components of tight junctions, adherens junctions, and the basement membrane were

Significance

Human cerebral small vessel disease (SVD) comprises age-associated intracerebral hemorrhages and global cognitive impairment, including vascular dementia. Human SVD presents in either familial or sporadic manifestation, involving either monogenic Mendelian defects or multitrait genetic variants. To better characterize the genetic and molecular mechanisms underlying SVD, appropriate animal models are needed. The *Srf*^{iECKO} mouse model presented here resembles human SVD pathology with regard to intracerebral hemorrhage formation and vascular dementia, including variability in onset and progression of cerebral symptoms. The Serum Response Factor (SRF)/Myocardin Related Transcription Factor (MRTF) are shown to regulate the expression of genes, which are essential for the maintenance of blood–brain barrier function and cerebral microvessel integrity. These findings suggest impairment of SRF/MRTF-mediated gene control as a molecular mechanism contributing to human SVD.

Author contributions: C.W., S.C.V., C.C., H.W., and A.N. designed research; C.W., S.C.V., H.R., C.S., C.C., H.W., S.M., and A.B. performed research; B.W., E.N.O., and R.H.A. contributed new reagents/analytic tools; C.W., S.C.V., H.W., A.B., A.D.G., R.H.A., B.J.P., and A.N. analyzed data; and C.W., S.C.V., and A.N. wrote the paper.

The authors declare no conflict of interest.

[1]To whom correspondence may be addressed. Email: alfred.nordheim@uni-tuebingen.de, christine.weinl@uni-tuebingen.de, or Eric.Olson@utsouthwestern.edu.

This article contains supporting information online at www.pnas.org/lookup/suppl/doi:10.1073/pnas.1509047112/-/DCSupplemental.

www.pnas.org/cgi/doi/10.1073/pnas.1509047112

down-regulated in brains of Srf^{iECKO} mice, identifying SRF/MRTF transcriptional control as a regulator of EC junction integrity.

Results

Lethal Brain Hemorrhaging upon Conditional EC-Specific Deletion of *Srf* in Postnatal and Adult Mice. Tamoxifen-induced EC-specific deletion of the *Srf* gene in Srf^{iECKO} animals elicited behavioral abnormalities (11) at varying times of onset, including reduced movement and lowered exploratory behavior after postnatal *Srf* deletion (Fig. S1). Mean survival of postnatally deleted animals was 17 d (Fig. 1*A*), irrespective of sex. Lethal symptoms included physical deterioration, hemiplegia, and ataxia. Brains dissected at age postnatal day 17 (P17) from postnatally deleted Srf^{iECKO} animals revealed multiple bleedings (Fig. 1*B*). Hemorrhages were observed as early as P6. All brain areas displayed hemorrhages, including cortex, hippocampus, and cerebellar lobes (Fig. S2). Bleedings were found only in postnatal brains and in no other organ investigated (Fig. S3).

When inducing EC-specific deletion of *Srf* in the adult, Srf^{iECKO} animals first displayed mild behavioral abnormalities in distinct initial phases of variable onset. Here, animals presented with hunched posture, ruffled fur, and long-legged walking motion. After an intermittent period of symptom-free behavior, animals entered an acute stage, displaying severe symptoms, including ataxia, hemiplegia, lethargy, and physical deterioration. Adult-deleted Srf^{iECKO} animals, but not control animals, showed reduced survival (Fig. 1*C*); both female and male animals were affected equally. Brain paraffin sectioning of affected adult animals revealed multiple locations of hemorrhage of different volume (Fig. 1*D*), likely causing the observed lethality. Microvessel bleeding occurred primarily in the brain rather than other organs, which may be explained by preferential expression of SRF in brain microvessels (12). Electron microscopic analysis of brain hemorrhages in both postnatally and adult-deleted animals revealed blood leakage into the surrounding brain tissue (Fig. 1 *E* and *F*). Whereas erythrocytes were confined to the lumen of ECs in control brains, red blood cells were found in the surrounding brain parenchyma in Srf^{iECKO} brains (Fig. 1 *E* and *F*). Tight junctions were found in both control and mutant brain vessels (Fig. 1 *E* and *F*).

At sites of hemorrhage in adult animals, vessel luminal content was released locally into the surrounding brain tissue, as revealed by tracing of the intraperitoneally applied dye Evans Blue (EB) (Fig. S4) and by detection of intracardially perfused Sulfo-NHS-LC-Biotin using streptavidin fluorescence (Fig. 2). Luminal content extravasation was seen in adult Srf^{iECKO} brains at spatially confined regions, most often in cortex and striatum (compare H&E-stained tissue sections) (Fig. 1*D*). High-resolution fluorescence images revealed both larger-volume hemorrhages (red circles) and microbleeds (white arrowheads). Kidney, an organ composed of fenestrated endothelium, served as positive control. No retinal fluorescence was seen (Fig. 2), congruent with our previous scanning laser ophthalmoscopy studies demonstrating absence of vascular dye leakage in Srf^{iECKO} retinae (11). Collectively, our data clearly reveal a requirement of endothelial SRF activity in both young and adult mice for maintenance of brain microvascular integrity.

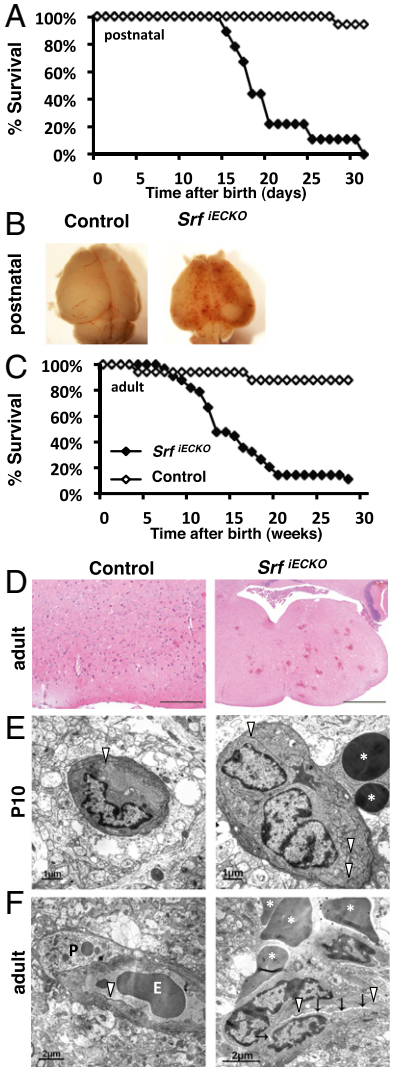

Fig. 1. Premature death and cerebral hemorrhages in Srf^{iECKO} animals. (*A*) Kaplan–Meier plot (percent survival) of control ($n = 16$) and Srf^{iECKO} ($n = 9$) animals upon postnatal *Srf* deletion. (*B*) Brains revealing hemorrhages in Srf^{iECKO} mice (P17). (*C*) Kaplan–Meier plot (percent survival) of control ($n = 16$) and Srf^{iECKO} ($n = 33$) animals upon adult *Srf* deletion. (*D*) H&E staining of adult control and Srf^{iECKO} brain sections, revealing multiple hemorrhages in Srf^{iECKO} brains (representative acute-stage animal shown). [Scale bars, 200 μm (*Left*) and 1,000 μm (*Right*).] (*E*) Electron microscopic images highlight intact blood vessels in P10 control animals and hemorrhages in Srf^{iECKO} brains. (Scale bars, 1 μm.) (*F*) Electron microscopic images highlight intact blood vessels in adult control animals and hemorrhages in Srf^{iECKO} brains. (Scale bars, 2 μm.) Arrows highlight obliterated vessel lumen; arrowheads point to tight junctions; white asterisks mark extravasated erythrocytes. E, intraluminal erythrocyte; P, pericyte.

In Vivo Time-Resolved Detection and Quantitation of Brain Hemorrhages and BBB Permeability Using MRI. To identify BBB disruption in vivo, Srf^{iECKO} and control animals were subjected to MRI, using T2-weighted imaging (T2WI) and contrast-enhanced T1-weighted imaging (T1WI). Multiple hemorrhages at various brain regions, not seen in control animals, were detected in adult-deleted Srf^{iECKO} mice at 24 wk of age (Fig. 3*A*). To monitor onset and progression of brain hemorrhage formation during the lifetime of Srf^{iECKO} mice, experimental animals were deleted for *Srf* at 6 wk of age and imaged longitudinally by T2WI every 2 wk from week 8 onward (normalized time point 1; nTP1) until the age of 24 wk (late time point; LTP). Clearly, hypointense lesions increased in number and distributed over entire brains of Srf^{iECKO} mice, which was not evidenced in controls (Fig. 3 *B*, *Upper*). Quantification (Fig. 3*C*) shows T2WI lesions to begin after week 12 of age and increase subsequently in most Srf^{iECKO} mice studied.

Subtracted T1WI measurements of Srf^{iECKO} mice, but not control animals, revealed the appearance of hyperintense diffuse lesions occurring in the entire brain (olfactory bulb, cortex, striatum, pons, and cerebellum) (Fig. 3 *B*, *Lower*). These lesions varied in number between animals and were mostly observed from week 12 onward (Fig. 3*D*). Individual lesions detected by T1WI occasionally disappeared during the course of MRI and—in some cases—recurred (Fig. 3*D*).

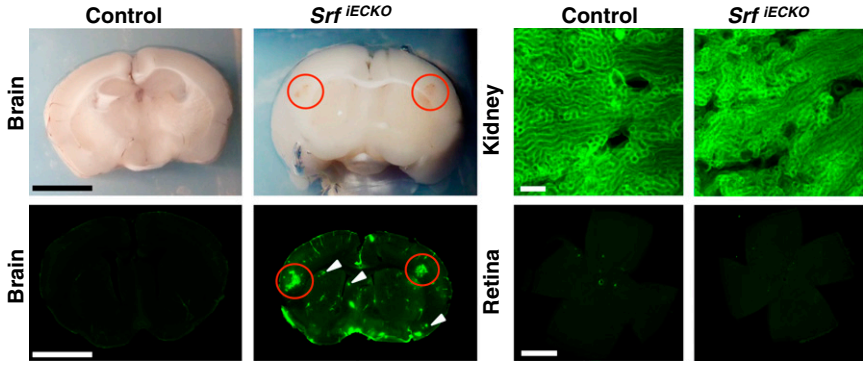

Fig. 2. Extravasation at localized sites of hemorrhage. Sulfo-NHS-LC-Biotin extravasations at localized sites of hemorrhage in Srf^{iECKO}, but not control brains, as visualized by blood coloring in brightfield (*Upper Left*) and fluorescence imaging (*Lower Left*) of an identical brain section. (Scale bars, 1 cm.) Red circles indicate larger-volume extravasations; white arrowheads indicate microbleeds. (*Upper Right*) Kidneys, composed of fenestrated endothelium, display constitutive dye extravasation. (Scale bar, 200 μm.) (*Lower Right*) Retinal flat-mounts evidence lack of extravasation in the retina ($n = 4$). (Scale bar, 1,000 μm.)

To quantify general BBB permeability and/or capillary leakage before and after appearance of T1WI lesions, we measured the percentage of global signal change elicited by contrast agent application (Fig. 3 *E* and *F*). There were significant differences in signal change between control and experimental animals at normalized time points nTP2, nTP3, and nTP4 and a nonsignificant trend at nTP1. Thus, MRI (both T2WI and T1WI) proved valuable to detect, localize, and quantify in vivo both onset and progression of hemorrhagic lesions. Furthermore, the T1WI study suggests that global changes in BBB permeability occur even before nTP4, the time point at which lesions were first identified macroscopically.

Adult Srf^{iECKO} Animals Recover Transiently from Initial Symptoms and Succumb Subsequently to Lethal Stroke. Brains of initial-stage animals revealed multifocal microhemorrhages with extravasation of erythrocytes (Fig. S5, *Center*), but no significant infiltration with macrophages or glial cells or activation of inflammation. Mild plasma extravasation (arrowheads) was visible by Periodic Acid Schiff (PAS) reactivity. The lack of Turnbull Blue staining in initial-stage brains indicated absence of older bleeds. Amyloid plaque formation—as seen in cerebral amyloid angiopathy (13)—was not detectable by Kongo Red staining in any of the tested animals. Furthermore, Nissl staining did not reveal signs of neuronal degeneration in mildly affected, initial-stage animals.

In contrast, in acute-stage animals, multiple sites of hemorrhage were associated with inflammation and infiltration of glial cells, as revealed by H&E staining (Fig. S5, *Right*). Prominent PAS-positive plasma extravasations displayed regions of Turnbull Blue staining (Fig. S5, *Right*), indicative of hemorrhages having occurred approximately several days before sample asservation. Neuronal degeneration was identified by cellular swelling, cytoplasmic vacuolization, nuclear chromatin condensation (karyopyknosis), and loss of Nissl substance (Fig. S5, *Right*).

SRF Cofactors MRTF, but Not TCF, Are Essential for a Functional Cerebral Endothelium. To identify SRF cofactors potentially required by SRF to ensure the integrity of postnatal and adult cerebral vasculature, we performed knockout studies on all five genes encoding known SRF cofactors—i.e., MRTFs (*Mrtf-a* and *Mrtf-b*) or TCFs (*Elk1*, *Elk3*, and *Elk4*). $Mrtf\text{-}a^{(-/-)}Mrtf\text{-}b^{iECKO}$ mice (11) showed hemorrhages of different volume, highly reminiscent of those displayed by Srf^{iECKO} mice (Fig. S6 *A* and *B*), strongly suggesting that MRTFs are the relevant endothelial SRF cofactors in vivo to ensure appropriate formation and functioning of the cerebral endothelium.

We next investigated the constitutive *Elk1*/*Elk4* double-knockout (14) and *Elk3* single-knockout mouse models (15). By analyzing the cerebral vasculature of both P10 and adult animals, no hemorrhages were observed in *Elk* knockout mouse brains (Fig. S6 *C*–*F*), demonstrating that TCF-type SRF cofactors Elk1, Elk3, and Elk4 were not required for formation and maintenance of the cerebral vasculature.

Srf^{iECKO} Cerebral Microvessels Have Impaired Basement Membrane Structure and Elevated Astrocyte Recruitment. Cerebral microvessel stability is dependent upon intact endothelial basement membrane structure and mural cell coverage. Regarding basement membrane structure, Collagen IV staining intensity was reduced on blood vessels of Srf^{iECKO} animals (P10) compared with control sections (Fig. 4*A*), in agreement with reduced Collagen IV (*Col4*) RNA levels in both postnatal and adult Srf^{iECKO} knockout brains (Fig. 5 *A* and *D*). Vessel coverage by vascular smooth muscle cells, investigated by using smooth muscle actin staining, was unchanged (Fig. 4*B*). Staining for glial fibrillary protein revealed an accumulation of activated astrocytes at locations of hemorrhaged blood vessels in Srf^{iECKO} brains (Fig. 4*C*). Importantly, no accumulation of astrocytes was evident near intact blood vessels in Srf^{iECKO} brains, indicating a specific astrocyte response to signals emanating from ruptured vessels in Srf^{iECKO} animals.

Reduced EC Junction Components in Srf^{iECKO} Brains. The integrity of the BBB depends on functional EC-connecting adherens junctions and tight junctions. We found that VE-Cadherin (*Cdh5*), a known SRF target gene encoding the main EC structural component of adherens junctions, was down-regulated in purified cerebral ECs from P10 Srf^{iECKO} animals, in close association with SRF depletion (Fig. S7). Regarding genes encoding tight junction proteins, Claudin1, 3, 5, and 12, as well as *ZO2* and *ZO3*, were significantly down-regulated in P10 whole brain tissue on the RNA level, whereas *ZO1* expression was not altered (Fig. 5*A*). Also, RNA expression of the basement membrane component *Col4* was reduced in Srf^{iECKO} whole brain tissue, whereas plasma lemma vesicle associated protein (*Plvap*), a marker for BBB breakdown (16), was significantly increased (Fig. 5*A*). Claudin5 protein expression was significantly down-regulated in adult Srf^{iECKO} brain lysates (Fig. 5 *B* and *C*). In acute-phase brain tissue of adult Srf^{iECKO} animals, RNA levels of vascular endothelial growth factor a (*Vegfa*), an indicator of hypoxia, were unchanged, whereas RNA levels of known SRF targets—namely, angiogenic receptor genes Vegfr-1 (*Flt1*) and Vegfr-2 (*Kdr*) and Smoothelin-b (*Smtn*)—were significantly down-regulated. RNA levels of the cerebral cavernous malformation genes *Ccm1* (*Krit1*), *Ccm2*, and *Ccm3*, as well as Lamininα3 (*Lama3*), were down-regulated (Fig. 5*D*).

We complemented the above tissue expression studies by analyses of cultured mouse ECs (mECs) transfected with siRNA against *Srf*. Here, we found that *Srf* and the SRF target genes β-actin (*Actb*), *Vegfr-1*, and *Vegfr-2* were significantly down-regulated, as well as the adherens junction components α-Actinin

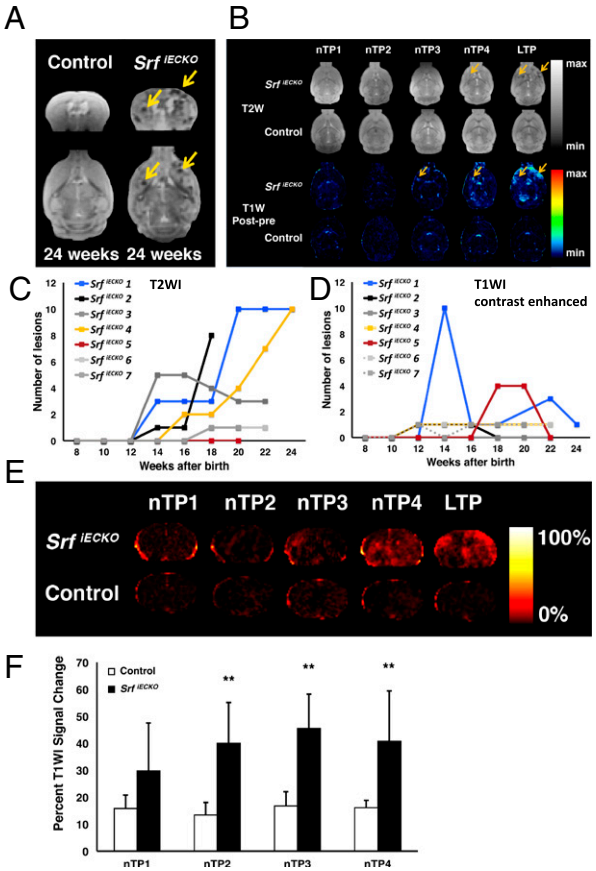

Fig. 3. Identification and quantification over time of hemorrhagic lesions and BBB permeability by MRI. (*A*) T2W MR images of control and Srf^{iECKO} animals, revealing stroke regions in Srf^{iECKO} animals (arrows), in coronal (*Upper*) and transversal (*Lower*) sections. (*B*) Transversal slides of T2WI (*Upper*) and T1WI (*Lower*) subtractions of Srf^{iECKO} and control animals. The T2WI of Srf^{iECKO} mice exemplifies the extent of hypointense signal produced by hemorrhages. Controls presented no lesions. Arrows point toward lesion areas. Time points of analysis (nTP and LTP) are defined in *SI Materials and Methods*. (*C* and *D*) Time course (from week 8 to 24) of presence of T2WI (*C*) and T1WI (*D*) lesions in seven individual animals, as exemplified for one animal in *B*, *Upper*. Mice 2 and 7 died after weeks 18 and 20 of age, respectively. (*E*) Global T1WI signal change, an indicator of BBB permeability, elicited upon contrast agent application. (*F*) Quantified percent global T1WI signal change at time points indicated in *E* was significant at nTP2, nTP3, and nTP4. Controls presented no significant signal change. Statistical analysis: Mauchly's test: no sphericity abnormalities ($P = 0.35$); ANOVA: significant overall difference ($P < 0.01$); Tukey's test: significant differences at nTP2, nTP3, and nTP4. $^{**}P < 0.01$. Data are presented as means ± SEM.

(*Actn*) and *Cdh5* and the tight junction component Claudin5 (Fig. 5*E*). Cofilin (*Cfl1*) served as negative control, and *Stat1* was used as an indicator of the IFN response associated with siRNA treatment, which was not induced in our experimental setup (Fig. 5*E*). Expression of *Ccm2* and *Ccm3*, but not *Ccm1*, was dependent on SRF expression (Fig. 5*E*). α-, β-, and γ-Catenin (*Ctnna*, *Ctnnb*, and *Ctnnc*, respectively) were unaffected. These findings suggest that the observed hemorrhages in brains of Srf^{iECKO} animals is due—at least in part—to impaired expression of EC junctional proteins, basement membrane components, or junction-associated proteins like CCMs, which were previously associated with stroke in murine and human systems (17).

Together, EC-specific *Srf* deletion results in multifocal hemorrhages, likely induced by a general weakening of the BBB due to transcriptional down-regulation of tight junction, adherens junction, and basement membrane structural proteins. The *Srf* mouse model serves as a genetic platform to study hemorrhagic stroke in a noninvasive manner—not requiring anesthesia or surgery—to explore strategies for early diagnoses and therapeutical treatments of BBB pathologies, including stroke.

Discussion

Human SVD accounts for at least 20% of all ischemic and hemorrhagic stroke (3), with intracerebral hemorrhage and microbleeds being vascular lesions serving as SVD markers (2, 3, 18). The genetic basis of human SVD-associated intracerebral hemorrhage is beginning to be understood, with autosomal-dominant single gene disorders being identified for the *APP* gene in cerebral amyloid angiopathy, the *COL4A1* gene in COL4A1-related intracerebral hemorrhage, and the *CCM* genes in stroke-prone cerebral cavernous malformations (18). In addition, non-Mendelian risk factors for hemorrhagic stroke associate with genomic loci encoding the *PMF1*/*SLC25A44*, *APOE*, and *COL4A2* genes (18). We demonstrate here that, in mice, independent null mutations in genes encoding the transcription factors SRF and MRTF-A/-B, but not Elk1, Elk3, and Elk4, cause lethal symptoms of hemorrhagic stroke. These symptoms are highly reminiscent of those observed in human patients suffering from SVD. We therefore hypothesize that deficiencies in SRF/MRTF activity may contribute to human intracerebral hemorrhage pathology. EC-specific *Srf* deletion in adult mice may serve as an animal model for cerebral microvascular dysfunction.

MRI has proven highly valuable in clinical human stroke management (3). Specifically, identification of cerebral microbleeds by T2*-weighted MRI has been associated with vessel fragility, blood extravasation, and future risk of primary or recurrent intracerebral hemorrhage (3, 4). Similarly, in Srf^{iECKO} animals, MRI analysis using both T2WI and contrast-enhanced T1WI allowed identification of microbleeds, intracerebral hemorrhages, and vessel permeability. T2WI allowed the detection and localization of microbleeds in Srf^{iECKO} animals, presenting as lesions of hypointense signal produced by superparamagnetic hemosiderin deposits (3, 19, 20) (Fig. 3*B*). Progressive temporal increase in microbleed number was generally observed (Fig. 3*C*), as described for human stroke patients (21). T2*-weighted images or Susceptibility Weighted Images are used clinically to identify microbleeds and are therefore recommended in future

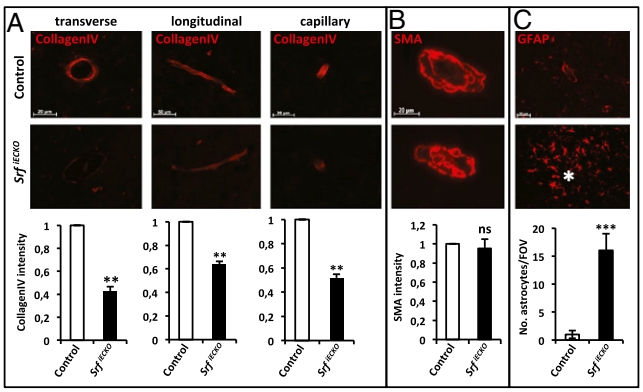

Fig. 4. Srf^{iECKO} cerebral microvessels show reduced collagen IV staining and elevated astrocyte recruitment. (*A*) Collagen IV staining of P10 cerebral microvessels in control (*Upper*) and Srf^{iECKO} (*Middle*) brains, as quantified by immunofluorescence signal intensity (*Lower*). (*Left*) Transverse section. (Scale bar, 20 μm.) (*Center*) Longitudinal section. (Scale bar, 50 μm.) (*Right*) Capillary. (Scale bar, 20 μm.) (*B*) Smooth muscle actin (SMA) staining of adult control (*Upper*) and Srf^{iECKO} (*Middle*) brains revealed no significant difference in smooth muscle cell presence (*Lower*). (Scale bar, 20 μm.) (*C*) Astrocytes stained by glial fibrillary acidic protein (GFAP) accumulate specifically around lesion sites in adult Srf^{iECKO} brains (*Middle*; hemorrhage highlighted by asterisk). Quantification of astrocyte number per field of view ($n = 5$; *Lower*). (Scale bar, 50 μm.) Data are presented as means ± SEM. $^{**}P < 0.01$; $^{***}P < 0.001$; ns, not significant.

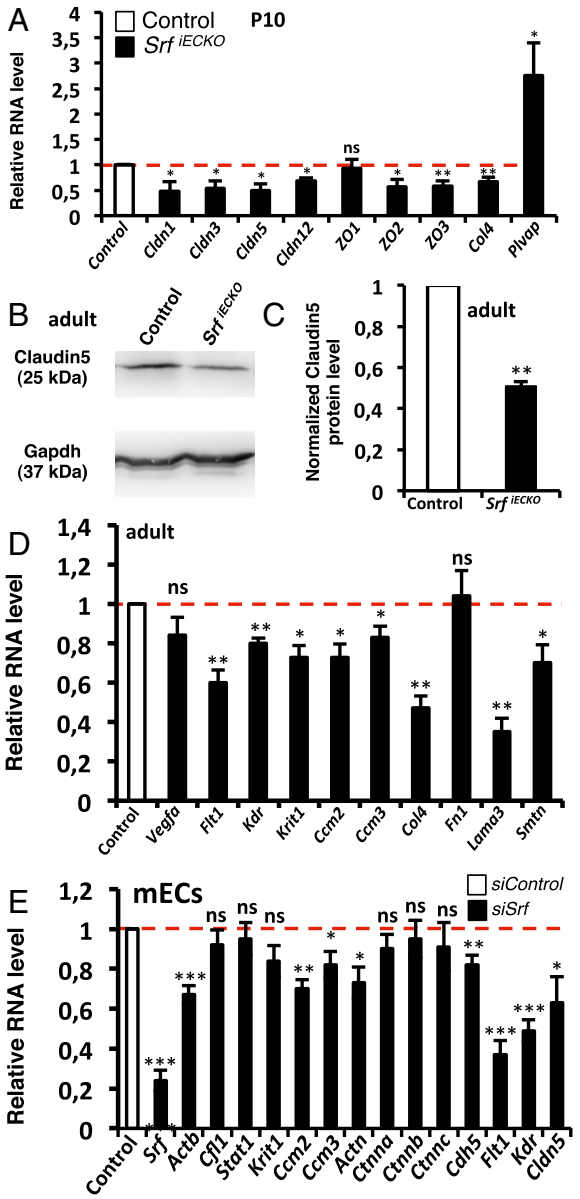

Fig. 5. Hemorrhaging correlates with down-regulation of tight junctions, adherens junctions, and basement membrane components. (*A*) Relative RNA levels (P10; whole brain) of tight junction components (Claudins and ZOs), Collagen IV, and Plvap in control vs. Srf^{iECKO} animals ($n > 5$). (*B*) Western blot (adult, whole brain) of control vs. Srf^{iECKO} animals for Claudin5 protein expression. Loading control: Gapdh. (*C*) Western blot quantitation (adult, whole brain) of Claudin5 in control vs. Srf^{iECKO} animals ($n = 3$). (*D*) Relative RNA levels of *Vegfa*, angiogenic receptors, different *Ccms*, and components of the basement membrane (adult, whole brain) of control vs. Srf^{iECKO} animals ($n > 5$). (*E*) mECs treated with control siRNA or siRNA against *Srf*; quantitative RT-PCR analysis ($n = 5$) for selected target genes. Data are presented as means ± SEM. $*P < 0.05$; $**P < 0.01$; $***P < 0.001$; ns not significant.

studies for better quantification of microbleed volumes. Microbleeds were also identified by Magnevist-enhanced T1WI (Fig. 3*B*), which revealed dynamic changes in signal over time (Fig. 3*D*), as also seen in human patients (22). The temporal changes of T1WI lesions might reflect the progression in behavioral phenotype of the animals, which displayed an initial mild-symptom stage and a recovery phase, followed by an acute lethal stage (Fig. 3 and Fig. S5).

Some T1WI lesions preceded the appearance of corresponding T2WI lesions at identical locations (Fig. 3*B*, differential arrow at nTP3). Such T1WI lesions may therefore indicate ongoing microbleeding during measurement. Indeed, Magnevist is a gadolinium-based contrast agent commonly used for detection of a disrupted BBB and/or abnormal vascularity (23, 24). Therefore, T1WI lesion distribution and pattern of appearance may reflect general small-vessel fragility in Srf^{iECKO} animals.

Such general vessel fragility may associate with vascular permeability in Srf^{iECKO} brains. Indeed, there are significant differences between control and Srf^{iECKO} animals at nTP2, nTP3, and nTP4. Even at nTP1, there is a trend for higher percent change in the Srf^{iECKO} (Fig. 3 *E* and *F*). This finding suggests that there is global increase of either contrast agent stagnancy or BBB permeability, with the latter allowing extravasation of contrast agent before and/or during vessel rupture. Global vessel permeability, as indicated by leakage of the low-molecular-weight MRI tracer Magnevist, was not revealed by EB or Sulfo-NHS-LC-Biotin staining, which only extravasated at localized points of vessel rupture (Fig. 2 and Fig. S4). This result may be due to these dyes forming high-molecular-weight complexes with blood components such as albumin. Together, our MRI data obtained with Srf^{iECKO} mice mirror human cerebral microbleeding and intracerebral hemorrhage (19, 22, 25), supporting the intriguing possibility that SRF deficiency may contribute to human hemorrhagic stroke pathology.

Human cerebral cavernous malformation associates with hemorrhagic stroke, in part caused by mutations in *CCM* genes (26). Interestingly, *Ccm1*, *Ccm2*, and *Ccm3* RNA levels were significantly decreased in brains of adult Srf^{iECKO} animals (Fig. 5*D*). However, we note the complete absence of cavernae in Srf^{iECKO} brains, indicating that Srf^{iECKO} mice do not provide a model of human cerebral cavernous malformation.

Microbleeds of Srf^{iECKO} mice are similarly found in human cerebral amyloid angiopathy (4), indicating a shared feature of vessel fragility. In cerebral amyloid angiopathy, amyloid plaques of neuronal origin deposited in the vessel wall are believed to cause this fragility (4, 27). However, no Kongo Red-positive amyloid plaques were observed in Srf^{iECKO} animals (Fig. S5), ruling out a common cause for microbleed formation in human cerebral amyloid angiopathy and Srf^{iECKO} mice.

Vessel hemorrhaging is likely caused by molecular defects in EC junction structures. First, regarding tight junction components, Claudins and ZO adapter proteins were down-regulated in Srf^{iECKO} brains. Murine genes encoding Claudin12 and ZO-2 are direct SRF/MRTF target genes, as shown for murine fibroblasts (7). Interestingly, $Cld5^{-/-}$ knockout mice show a size-selective BBB permeability (28). Second, regarding adherens junction components, the *Cdh5* gene was identified as a direct SRF target gene (11, 12). In line, mouse embryos lacking *Cdh5* die at embryonic day 9.5 (E9.5) (29), and disruption of *Cdh5* in the adult murine vasculature causes hemorrhaging (29, 30). The adherens junction component *Actn*, down-regulated in SRF-deficient mECs (Fig. 5*E*), may be regulated indirectly by SRF. Third, both tight junctions and adherens junctions derive mechanical strength by linkage to cytoskeletal actin microfilaments (5). Actin genes are prototypical SRF/MRTF target genes (8) and *Actb* RNA was down-regulated in SRF knockdown mECs (Fig. 5*E*). Fourth, reduced levels of basement membrane proteins may cause small vessel fragility. Indeed, expression of the *Col4* gene (encoding Collagen typeIV) was reduced in Srf^{iECKO} P10 brains at RNA (Fig. 5*A*) and protein (Fig. 4) level and at RNA level in adult Srf^{iECKO} brains (Fig. 5*D*). Interestingly, mutant *Col4a1* mice display intracerebral hemorrhage (31), similar to Srf^{iECKO} animals. In some human SVD patients with intracerebral hemorrhage, mutations in *COL4A1* and *COL4A2* are found (18, 31), as well as *COL4A2* polymorphisms in sporadic intracerebral hemorrhage (32). Thus, the correlation of intracerebral hemorrhage occurrence and Collagen IV deficiency is shared between $Col4a1^{(-/-)}$ mice, Srf^{iECKO} mice, and some human SVD patients.

In conclusion, Srf^{iECKO} and $Mrtf\text{-}a^{(-/-)}Mrtf\text{-}b^{iECKO}$ mice identify the SRF/MRTF transcriptional control module as an essential regulator of cerebral microvascular integrity. The entire assembly

of EC junction components—including tight junctions, adherens junctions, their linked actin cytoskeleton, and the basement membrane—are built from key structural proteins encoded by SRF/MRTF target genes. Consistently, SRF/MRTF deficiency in murine ECs causes small vessel fragility and brain hemorrhage. Although Srf^{iECKO} mice demonstrate the essential role of SRF/MRTF in cerebral microvessel stability, SRF/MRTF might fulfill a similar function in the human brain. Accordingly, some hemorrhagic stroke-associated human conditions may be caused by impaired SRF/MRTF activity. Thus, we speculate that the increase in hemorrhagic incidence associated with increasing age of mice (33) and human patients (34) might have a common underlying basis in age-dependent down-regulation of SRF/MRTF activity, potentially exerted either by epigenetic mechanisms (35) reducing SRF/MRTF expression or posttranslational mechanisms impairing SRF/MRTF function (36).

Materials and Methods

Mouse Models. Srf^{iECKO} and $Mrtf\text{-}a^{(-/-)}Mrtf\text{-}b^{iECKO}$ mice were generated as described (11). Induction of deletion by Tamoxifen is described in *SI Materials and Methods*. *Elk1/Elk4* double-knockout (14) and *Elk3* knockout (15) animals were bred as described. Genotyping was performed by PCR of ear biopsies. All animal experiments were approved by the Regierungspraesidium Tuebingen (Germany).

EC Culture and siRNA Treatment. Immortalized mECs were cultured and transfected (11, 37) as described in *SI Materials and Methods*.

RNA Isolation, cDNA Synthesis, and Semiquantitative RT-PCR. For description of methods regarding RNA isolation, cDNA synthesis, and semiquantitative RT-PCR (38), see *SI Materials and Methods*.

Western Blotting. Brain tissue was lysed in radioimmunoprecipitation assay buffer, and SRF and Claudin5 protein levels were detected by Western blotting (11, 39), as described in *SI Materials and Methods*.

MRI. MR images were acquired by using a Clinscan 7T MR scanner (Bruker Biospin) using a four-channel mouse brain surface coil. For detailed imaging protocols, data analysis, and statistics, see *SI Materials and Methods*.

Histological H&E and Immunohistochemistry. For details regarding H&E staining, immunohistochemistry, microscopic analysis, and signal quantitation, see *SI Materials and Methods*.

Sulfo-NHS-LC-Biotin Labeling. For staining of luminal protein content and localization of sites of extravasation, Sulfo-NHS-LC-Biotin labeling (40) is described in *SI Materials and Methods*.

Statistics. Values are presented as means ± SEM. For comparison of different experiments, values are normalized to the control = 1 or 100%. To test significance, Student's *t* tests were used; $P < 0.05$ was considered statistically significant.

ACKNOWLEDGMENTS. We thank R. Treisman for providing *Elk1(-/0)::Elk4(−/−)* dKO mice, G. Frommer-Kästle for help with electron microscopy, S. Alberti for advice on animal experimentation, and U. Ehrnemann and A. Pagenstecher for clinical advice. C.W. and A.N. were supported by the Dr. Karl-Kuhn-Foundation and Deutsche Forschungsgemeinschaft No120/12-4.

1. Go AS, et al.; American Heart Association Statistics Committee and Stroke Statistics Subcommittee (2013) Executive summary: Heart disease and stroke statistics–2013 update: A report from the American Heart Association. *Circulation* 127(1):143–152.
2. Haffner C, Malik R, Dichgans M (April 22, 2015) Genetic factors in cerebral small vessel disease and their impact on stroke and dementia. *J Cereb Blood Flow Metab*, 10.1038/jcbfm.2015.71.
3. Wardlaw JM, Smith C, Dichgans M (2013) Mechanisms of sporadic cerebral small vessel disease: Insights from neuroimaging. *Lancet Neurol* 12(5):483–497.
4. Yates PA, et al. (2014) Cerebral microbleeds: A review of clinical, genetic, and neuroimaging associations. *Front Neurol* 4:205.
5. Daneman R, Prat A (2015) The blood-brain barrier. *Cold Spring Harb Perspect Biol* 7(1):a020412.
6. Cen B, Selvaraj A, Prywes R (2004) Myocardin/MKL family of SRF coactivators: Key regulators of immediate early and muscle specific gene expression. *J Cell Biochem* 93(1):74–82.
7. Esnault C, et al. (2014) Rho-actin signaling to the MRTF coactivators dominates the immediate transcriptional response to serum in fibroblasts. *Genes Dev* 28(9):943–958.
8. Olson EN, Nordheim A (2010) Linking actin dynamics and gene transcription to drive cellular motile functions. *Nat Rev Mol Cell Biol* 11(5):353–365.
9. Posern G, Treisman R (2006) Actin' together: Serum response factor, its cofactors and the link to signal transduction. *Trends Cell Biol* 16(11):588–596.
10. Franco CA, et al. (2013) SRF selectively controls tip cell invasive behavior in angiogenesis. *Development* 140(11):2321–2333.
11. Weinl C, et al. (2013) Endothelial SRF/MRTF ablation causes vascular disease phenotypes in murine retinae. *J Clin Invest* 123(5):2193–2206.
12. Franco CA, et al. (2008) Serum response factor is required for sprouting angiogenesis and vascular integrity. *Dev Cell* 15(3):448–461.
13. Winkler DT, et al. (2001) Spontaneous hemorrhagic stroke in a mouse model of cerebral amyloid angiopathy. *J Neurosci* 21(5):1619–1627.
14. Costello P, et al. (2010) Ternary complex factors SAP-1 and Elk-1, but not net, are functionally equivalent in thymocyte development. *J Immunol* 185(2):1082–1092.
15. Weinl C, et al. (2014) Elk3 deficiency causes transient impairment in post-natal retinal vascular development and formation of tortuous arteries in adult murine retinae. *PLoS One* 9(9):e107048.
16. Shue EH, et al. (2008) Plasmalemmal vesicle associated protein-1 (PV-1) is a marker of blood-brain barrier disruption in rodent models. *BMC Neurosci* 9:29.
17. Cunningham K, et al. (2011) Conditional deletion of Ccm2 causes hemorrhage in the adult brain: A mouse model of human cerebral cavernous malformations. *Hum Mol Genet* 20(16):3198–3206.
18. Falcone GJ, Malik R, Dichgans M, Rosand J (2014) Current concepts and clinical applications of stroke genetics. *Lancet Neurol* 13(4):405–418.
19. Roob G, et al. (2000) Frequency and location of microbleeds in patients with primary intracerebral hemorrhage. *Stroke* 31(11):2665–2669.
20. Tong KA, et al. (2008) Susceptibility-weighted MR imaging: A review of clinical applications in children. *AJNR Am J Neuroradiol* 29(1):9–17.
21. Martinez-Ramirez S, Greenberg SM, Viswanathan A (2014) Cerebral microbleeds: Overview and implications in cognitive impairment. *Alzheimers Res Ther* 6(3):33.
22. Lee SH, et al. (2011) Dynamic temporal change of cerebral microbleeds: Long-term follow-up MRI study. *PLoS One* 6(10):e25930.
23. Hynynen K, McDannold N, Vykhodtseva N, Jolesz FA (2001) Noninvasive MR imaging-guided focal opening of the blood-brain barrier in rabbits. *Radiology* 220(3):640–646.
24. Tsushima Y, Aoki J, Endo K (2003) Brain microhemorrhages detected on T2*-weighted gradient-echo MR images. *AJNR Am J Neuroradiol* 24(1):88–96.
25. Fisher M, French S, Ji P, Kim RC (2010) Cerebral microbleeds in the elderly: A pathological analysis. *Stroke* 41(12):2782–2785.
26. Richardson BT, Dibble CF, Borikova AL, Johnson GL (2013) Cerebral cavernous malformation is a vascular disease associated with activated RhoA signaling. *Biol Chem* 394(1):35–42.
27. Biffi A, Greenberg SM (2011) Cerebral amyloid angiopathy: A systematic review. *J Clin Neurol* 7(1):1–9.
28. Nitta T, et al. (2003) Size-selective loosening of the blood-brain barrier in claudin-5-deficient mice. *J Cell Biol* 161(3):653–660.
29. Carmeliet P, et al. (1999) Targeted deficiency or cytosolic truncation of the VE-cadherin gene in mice impairs VEGF-mediated endothelial survival and angiogenesis. *Cell* 98(2):147–157.
30. Corada M, et al. (1999) Vascular endothelial-cadherin is an important determinant of microvascular integrity in vivo. *Proc Natl Acad Sci USA* 96(17):9815–9820.
31. Gould DB, et al. (2006) Role of COL4A1 in small-vessel disease and hemorrhagic stroke. *N Engl J Med* 354(14):1489–1496.
32. Rannikmäe K, et al.; METASTROKE Consortium; CHARGE WMH Group; ISGC ICH GWAS Study Collaboration; WMH in Ischemic Stroke GWAS Study Collaboration; International Stroke Genetics Consortium (2015) Common variation in COL4A1/COL4A2 is associated with sporadic cerebral small vessel disease. *Neurology* 84(9):918–926.
33. Toth P, et al. (2015) Aging exacerbates hypertension-induced cerebral microhemorrhages in mice: Role of resveratrol treatment in vasoprotection. *Aging Cell* 14(3):400–408.
34. Bokura H, et al. (2011) Microbleeds are associated with subsequent hemorrhagic and ischemic stroke in healthy elderly individuals. *Stroke* 42(7):1867–1871.
35. Pearce WJ (2011) Epigenetics: An expanding new piece of the stroke puzzle. *Transl Stroke Res* 2(3):243–247.
36. Collard L, et al. (2014) Nuclear actin and myocardin-related transcription factors control disuse muscle atrophy through regulation of Srf activity. *J Cell Sci* 127(24):5157–5163.
37. Benedito R, et al. (2009) The notch ligands Dll4 and Jagged1 have opposing effects on angiogenesis. *Cell* 137(6):1124–1135.
38. Weinhold B, et al. (2000) Srf(-/-) ES cells display non-cell-autonomous impairment in mesodermal differentiation. *EMBO J* 19(21):5835–5844.
39. Koegel H, et al. (2009) Loss of serum response factor in keratinocytes results in hyperproliferative skin disease in mice. *J Clin Invest* 119(4):899–910.
40. Wang Y, et al. (2012) Norrin/Frizzled4 signaling in retinal vascular development and blood brain barrier plasticity. *Cell* 151(6):1332–1344.